Spin-wave dynamics in nonlinear chains with spin-lattice interactions

M. O. Sales,[1] A. Ranciaro Neto,[2] and F. A. B. F. de Moura[3]

[1]*IFMA Campus São João dos Patos, rua Padre Santiago, s/n, Centro, São João dos Patos-MA 65665-000, Brazil*

[2]*Faculdade de Economia, Administração e Contabilidade, Universidade Federal de Alagoas, Maceió AL 57072-970, Brazil*

[3]*Instituto de Física, Universidade Federal de Alagoas, Maceió AL 57072-970, Brazil*

(Received 11 October 2018; published 26 December 2018)

We consider the one-magnon subspace of a quantum Heisenberg Hamiltonian with ferromagnetic ground state. In this model, the spins belong to a chain which contains a cubic interaction between the nearest neighbors atoms. The quantum Heisenberg spin-spin coupling is a function of the distance between them. By providing a numerical solution of the Heisenberg nonlinear lattice model, we found that magnon-lattice coupling affects the magnon dynamics in distinct ways: for a specific range of magnon-lattice interaction values, a magnon-soliton pair is observed. Moreover, an effective repulsion between the magnon's excitation and the lattice deformation is noticed for other cases.

DOI: 10.1103/PhysRevE.98.062136

I. INTRODUCTION

Time-dependent behavior of an initially localized electronic wave packet has a direct connection with the transport properties of materials [1]. Anderson and co-workers have shown that the presence of static disorder is a relevant issue that narrows the spatial extension of the wave function [2]. They demonstrated that, even in mild disorder degree, a system with dimensions below two has all eigenstates localized in a finite fraction of the lattice: a set of results usually named Anderson localization theory (ALT) [1–4]. In the context of theoretical models with time-dependent intrinsic disorder, we remind one of the effective model that takes into account the interaction between electrons and optical phonons [5–7]. This kind of system is well described by a nonlinear Schrödinger equation [5,6] with time-dependent diagonal disorder (the on-site potential is, in general, the square modulus of the wave function [5,6]). An interesting phenomenon associated to nonlinearity is self-trapping (ST), which occurs when the nonlinearity strength exceeds a critical value of the order of the bandwidth [7–12]. In general, the ST phenomenon is characterized by the localization of the wave packet around its initial position. Moreover, in Refs. [13–25] Velarde and co-workers demonstrated the existence of a polaron-soliton quasiparticle in nonlinear lattices and they also showed its importance to charge carrying. The pair formation with self-trapped states (polaron states) and the lattice solitons has been generally termed as solectron [13–24]. We emphasize that the solectron theory represents an interesting generalization of the original polaron concept which mediates non-Ohmic supersonic electric conduction [21]. The electronic transport mediated by nonlinear effect was observed in several two-dimensional anharmonic lattices along crystallographic axes, particularly in a square lattice similar to the cuprate alloy [24].

In this work we investigate the interaction between a magnon excitation and the nonlinear lattice vibrations. We consider a subspace of a single spin deviation (one-magnon framework) in a quantum Heisenberg Hamiltonian with the ferromagnetic ground state. The spin chain contains an intrinsic cubic interaction. Magnon excitations and the spin vibrations interact with each other as a function of the distance between the spins. By solving numerically the Heisenberg-nonlinear lattice model, we find that the magnon-lattice coupling intensity (α) promotes distinct dynamics. For a range of values of α, it is noticed an occurrence of a magnon-soliton pair similar to the solectron which was in the previous works of Velarde and co-workers [13–25]. However, our calculations also suggest a new and counterintuitive behavior associated with the Heisenberg-nonlinear lattice model: there is numerical evidence that points to a kind of effective repulsion between the magnon and the lattice deformation.

II. MODEL AND NUMERICAL CALCULATION

Our approach consists of a quantum ferromagnetic Heisenberg model with N spins $1/2$ under the effect of nonlinear lattice vibrations. The quantum Hamiltonian describing the spin waves can be written as [3,4]

$$\mathcal{H}_S = -\sum_{j=1}^{N}\{J_{j,j+1}\vec{S}_j\vec{S}_{j+1}\}, \tag{1}$$

where $J_{j,j+1}$ represents the exchange couplings connecting sites j and $j+1$. In our model, $J_{j,j+1}$ depends upon spin displacement $\{Q_j\}$ from their equilibrium position: $J_{j,j+1} = e^{-\alpha(Q_{j+1}-Q_j)}$. Here, α is an intensity parameter of spin-spin coupling energy. This quantity has the same status of the "electron-phonon" coupling presented in Refs. [21,26]. In the present model, α is also a measure of the intensity of (spin-wave)-lattice coupling. A nonlinear classical Hamiltonian H_L is considered in order to describe the spin vibrations:

$$H_L = \sum_{j=1}^{N}\frac{P_j^2}{2m_j} + \sum_{j=1}^{N}\left(\frac{1}{4}[(Q_{j+1}-Q_j)^2 + (Q_j-Q_{j-1})^2] + \frac{\eta}{6}[(Q_{j+1}-Q_j)^3 + (Q_j-Q_{j-1})^3]\right), \tag{2}$$

where P_j is the momentum of the spin at site (j) and $m_j = 1$ in all calculations. Our interest lies in studying the one-magnon subspace of the Hamiltonian in Eq. (1). The typical time-dependent wave function of such excitation is given by $|\Psi(t)\rangle = \sum_j c_j|j\rangle$ where $|j\rangle$ represents a wave function of the chain state with a single reversed spin at site j ($|j\rangle = S_j^-|0\rangle$ where $|0\rangle$ is the ferromagnetic ground state). The time-dependent Schrödinger equation is written as

$$i\frac{dc_j(t)}{dt} = (J_{j-1,j} + J_{j,j+1})\frac{c_j(t)}{2} - J_{j-1,j}\frac{c_{j-1}(t)}{2} - J_{j,j+1}\frac{c_{j+1}(t)}{2}, \tag{3}$$

The classical spins vibrations can be obtained through the Hamilton equation

$$\begin{aligned}\frac{d^2Q_j}{dt^2} &= (Q_{j+1} + Q_{j-1} - 2Q_j) \\ &+ \eta[(Q_{j+1} - Q_j)^2 - (Q_j - Q_{j-1})^2] \\ &+ \frac{\alpha}{2}[e^{-\alpha(Q_j - Q_{j-1})}(c_j^* c_j + c_{j-1}^* c_{j-1}) \\ &- e^{-\alpha(Q_{j+1} - Q_j)}(c_j^* c_j + c_{j+1}^* c_{j+1}) \\ &+ e^{-\alpha(Q_{j+1} - Q_j)}(c_{j+1}^* c_j + c_j^* c_{j+1}) \\ &- e^{-\alpha(Q_j - Q_{j-1})}(c_{j-1}^* c_j + c_j^* c_{j-1})].\end{aligned} \tag{4}$$

Equations (3) and (4) are solved as follows: (i) The time evolution operator $\tilde{O}(\delta t)$ is obtained using a high-order Taylor expansion $\tilde{O}(\delta t) = e^{(-iH_S\delta t)} = 1 + \sum_{l=1}^{n_o}(-iH_S\delta t)^l/(l!)$ [27]; the quantum state $|\Psi(t+\delta t)\rangle$ is described as $|\Psi(t+\delta t)\rangle = \tilde{O}(\delta t)|\Psi(t)\rangle$. (ii) We solve classical equations using a predictor-corrector Euler method defined as follows [26,28]: (a) first we calculate a prediction $Q_j(\delta t)^* \approx Q_j(t=0) + \delta t[(dQ_j/dt)|_{t=0}$ at time δt. (b) Then, we apply a correction formula in order to get improved solutions $Q_j(\delta t)^*$, i.e., $Q_j(\delta t) \approx Q_j(t=0) + (\delta t/2)[(dQ_j/dt)|_{t=0} + (dQ_j^*/dt)|_{\delta t}]$. In our calculations this correction formula was used three times. The sum of the evolution operator was truncated at $n_o = 12$ and $\delta t = 10^{-2}$. The wave-function norm within the entire integration was kept within numerical tolerance ($|1 - \sum_j |c_j(t)|^2| < 10^{-8}$). We also compare our simulations with those obtained by using a standard integrator [e.g., fourth-order Runge-Kutta (RK4) [28]]. The results obtained by both methods do not show any qualitative difference; however, the Taylor-Euler procedure requires less computational time. In order to monitor the magnon dynamics we use some standard tools, namely, the magnon's mean position $\langle n\rangle_S(t)$ and the participation number $\xi(t)$, respectively:

$$\langle n\rangle_S(t) = \sum_j (j - j_0)|c_j(t)|^2, \tag{5}$$

$$\xi(t) = \frac{\sum_j |c_j(t)|^2}{\sum_j |c_j(t)|^4}. \tag{6}$$

We emphasize that the lattice behavior at the jth site will be also investigated by analyzing the quantity A_j defined as a kind of generalized probability of local deformation around site j. This quantity is obtained as follows: First, we compute the quantity $u_j = (1 - e^{[-Q_j + Q_{j-1}]})^2$. Second, we normalize u_j to get the generalized probability of local deformation A_j, i.e., $A_j = u_j/\sum_j(u_j)$. Using A_j we can compute the centroid $\langle n\rangle_L(t)$ of the lattice deformation as

$$\langle n\rangle_L(t) = \sum_j (j - j_0)A_j. \tag{7}$$

We emphasize that $\langle n\rangle_S(t)$ and $\langle n\rangle_L(t)$, respectively, represent the centroid for time t of the magnon and the lattice deformation. The participation function $\xi(t)$ provides an estimate of the number of sites under which the wave packet is spread at time t.

III. RESULTS

Most of the calculations were done in a very large chain with $N = 5 \times 10^4$ sites. At $t = 0$, the j_0th spin was deviated [here $j_0 = N/2$, then $c_j(t=0) = \delta_{j,N/2}$] and lattice deformations were set to $Q_j(t=0) = 0$ and $\dot{Q}_j(t=0) = \delta_{j,N/2}$, thus promoting the appearance of a solitonic mode within this chain [21,26]. We emphasize that only a finite fraction of the initial energy is participating in the solitoniclike lattice deformation; the other part evolves along the chain through nonlinear vibrational modes also called radiation [29]. We stress that numerical integration of the quantum and classical equations was done initially in a small fraction of the complete chain. Our simulation starts with j restricted to the range $j_0 - N^* < j < j_0 + N^*$ with $N^* = 200$. Whenever the wave function or the atomic vibration arrives at the boundaries of the initial chain, N^* is automatically increased by ten sites. By using this trick, called self-expanded chain, we avoid any unwanted border effects.

In Figs. 1(a)–1(c), we plot the magnon's mean position $[\langle n\rangle_S(t)]$ versus t for $\eta = 1$ and $\alpha = 0.0$ up to 2.8. We observed that with the absence of a magnon-lattice interaction ($\alpha = 0$) we found $\langle n\rangle_S(t) = 0$, i.e., the mean position of the spin deviations remains localized at the initial site. This result is in a good agreement with previous calculations [3,4]. For $\alpha > 0$, we found an interesting and new behavior: the magnon's position changeed drastically with α; moreover we also observed that the direction of movement also depends of α. For $0 < \alpha < 2$, the magnon's mean position is positive $[\langle n\rangle_S(t) > 0]$ thus indicating that the magnon's wave packet moves from the center to the right side of the chain. For $\alpha \geqslant 2$ we found $\langle n\rangle_S(t) < 0$ (magnon excitation moves from the center to the left side of the chain). Therefore, numerical simulation suggests that the dynamics of one magnon in a ferromagnetic chain may be controlled by the spin-lattice coupling. These results (see Fig. 1) deserve a more detailed description. In Fig. 2 we plot the participation number (ξ_+ and ξ_-) versus time (t) for $\eta = 1$ and $\alpha = 0.4$. We stress that for $\alpha = 0.4$ the magnon moves to the right side [see Fig. 1(a)]. We emphasize that ξ_+ and ξ_- were both computed using Eq. (6) with a change at the range of sum in j: $j_0 \leqslant j \leqslant N$ for ξ_+ and $1 \leqslant j \leqslant j_0$ for ξ_-. Hence, ξ_+ represents the spread of the wave packet at the right side of the chain (i.e., $j \geqslant j_0$) and ξ_- represents the size of the wave packet at the left side of the chain (i.e., $j \leqslant j_0$). We clearly observed that ξ_- is larger than ξ_+. In previous works [19,21], this kind of behavior was associated with the asymmetric behavior of the wave packet due to the electron-phonon interaction. In brief, a portion of

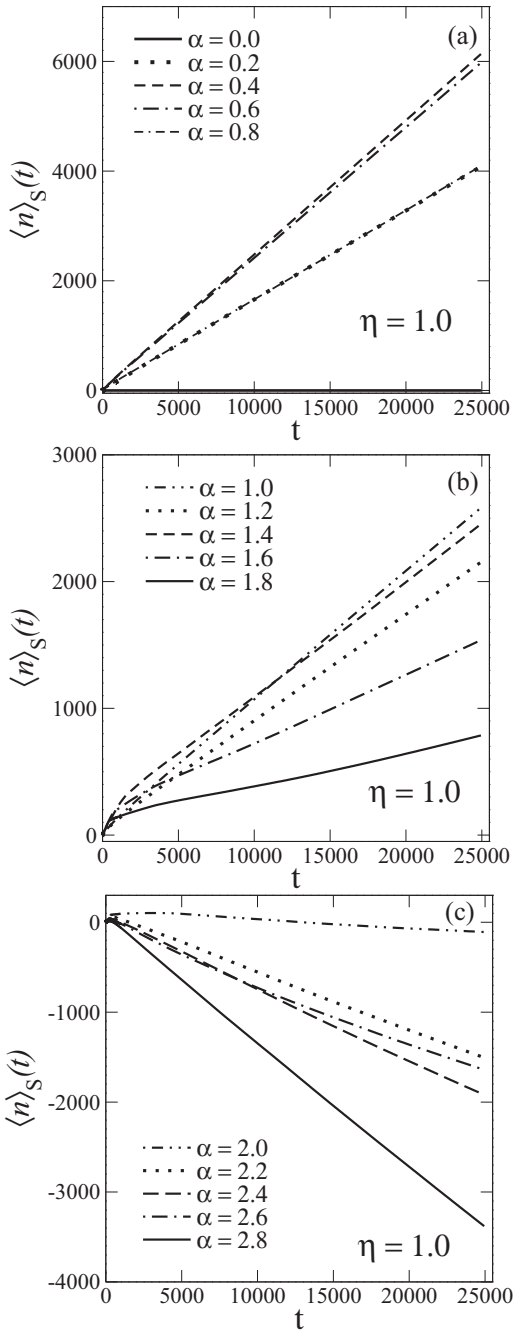

FIG. 1. Magnon's centroid $[\langle n\rangle_S(t)]$ versus t for $\eta = 1$ and $\alpha = 0.0$ up to 2.8. For $\alpha < 2$, the magnon exhibits a displacement from the center to the right side of the chain. For $\alpha \geqslant 2$, our results $[\langle n\rangle_S(t) < 0]$ suggest an inversion on the direction of movement.

the wave packet becomes trapped at the positive side ($j > j_0$) by a solitonic mode and, therefore, the wave packet's spread at this side indeed decreases.

This hypothesis may be confirmed in our work by analyzing the mean position of the wave packet and the lattice deformation [i.e., respectively $\langle n\rangle_S(t)$ and $\langle n\rangle_L(t)$]. In Figs. 3(a)–3(d), we plot $\langle n\rangle_S(t)$ and $\langle n\rangle_L(t)$ versus time for several values of $\alpha = 0.4$ up to 2.8. In Fig. 3(a) we notice that the solitonic deformations and the wave packet moves roughly together. Therefore, the results found in Fig. 3(a)

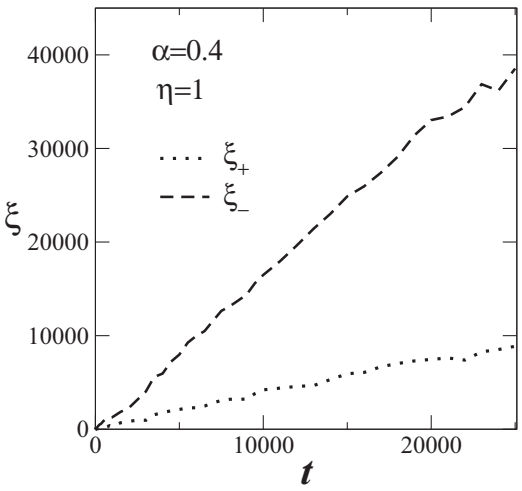

FIG. 2. The participation number (ξ_+ and ξ_-) versus time (t) for $\eta = 1$ and $\alpha = 0.4$. We notice that ξ_- is larger than ξ_+, thus confirming the asymmetric propagation of the wave packet.

explain qualitatively the asymmetric behavior found in Fig. 2 and also the behavior of the magnon excitation for this case: the solitonic mode traps a finite fraction of the initial wave packet and they move together; moreover, this magnon-soliton pair for $\alpha = 0.4$ seems to dominate the dynamics within the chain. However, in Figs. 3(b)–3(d) we clearly observe a distinct range of dynamics behavior. The lattice and magnon dynamics are separated. For large values of α, our calculations suggest indeed a kind of repulsion between the magnon and the lattice deformation [see Figs. 3(c) and 3(d)]. By analyzing the possibility of magnon-soliton coupling according to previous references [19,21], this is a counterintuitive result. In Figs. 4(a)–4(d), we plot the wave-packet component $|c_j(t)|^2$ [Figs. 4(a) and 4(b)] and the lattice deformation A_j Figs. 4(c)

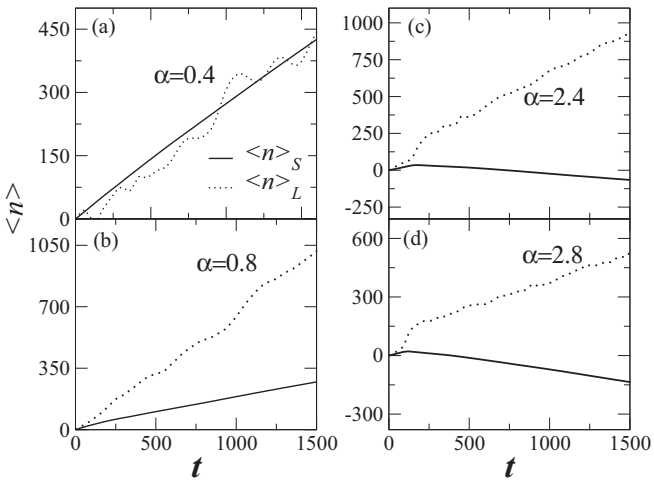

FIG. 3. Mean position of the magnon $[\langle n\rangle_S(t)]$ and lattice deformation $[\langle n\rangle_L(t)]$ versus time for several values of $\alpha = 0.4$ up to 2.8. In (a) our results suggest the existence of a kind of magnon-soliton pair moving along the chain. However, in (b)–(d) our calculations suggest that the magnon wave packet and the lattice are moving in separate ways.

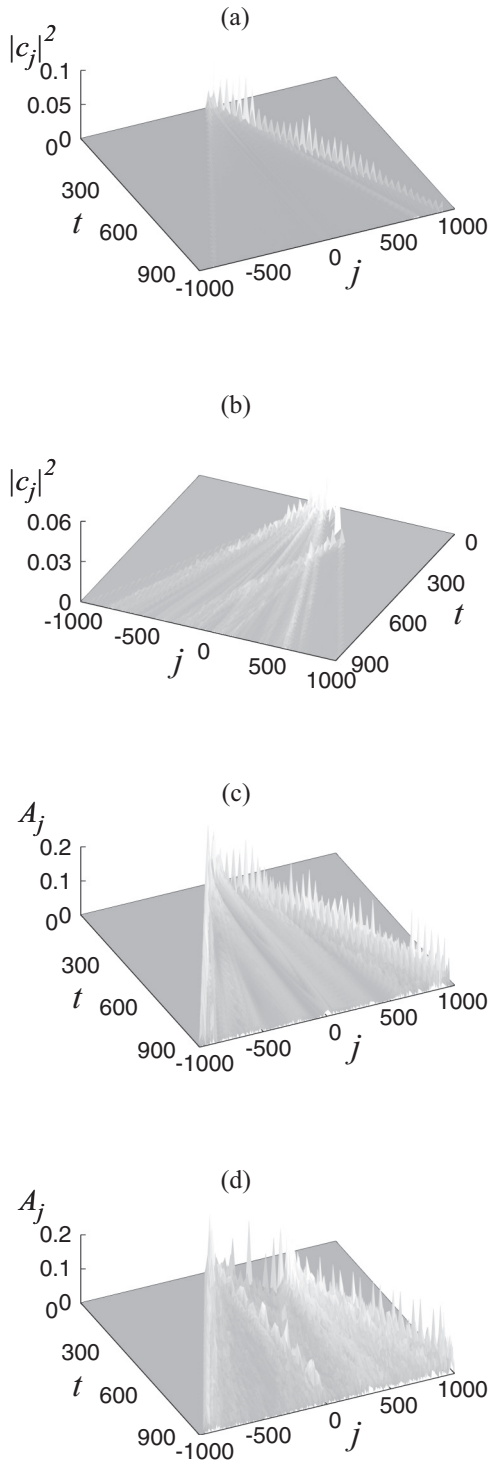

FIG. 4. Square modulus of the wave function $|c_j(t)|^2$ [(a),(b)] and the lattice deformation A_j [(c),(d)] versus j and t for $\eta = 1$, $\alpha = 0.4$ [(a),(c)] and $\alpha = 2.8$ [(b),(d)].

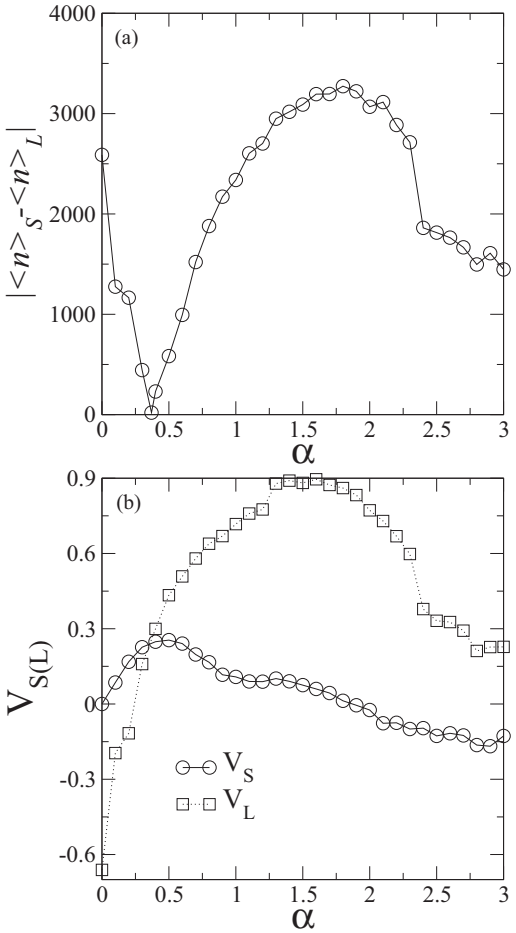

FIG. 5. (a) Our calculations for the mean distance between the magnon and the lattice deformation $|\langle n_S\rangle - \langle n_L\rangle|$ versus the magnon-lattice interaction (α). The magnon and the lattice deformation mean the position obtained where $\langle n_S\rangle = \langle n\rangle_S(t \to 4 \times 10^3)$ and $\langle n_L\rangle = \langle n\rangle_L(t \to 4 \times 10^3)$. (b) The velocity of the magnon (V_S) and the lattice deformation (V_L) versus (α). Calculations of the velocity were done by doing a linear regression of the quantities $\langle n\rangle_S(t)$ and $\langle n\rangle_L(t)$ for long time.

and 4(d)] versus j and t for $\eta = 1$, $\alpha = 0.4$ [Figs. 4(a) and 4(c)] and 2.8 [Figs. 4(b) and 4(d)]. Also, for $\alpha = 0.4$ the magnon and the lattice deformation seems to move together with approximately the same velocity [see Figs. 4(a) and 4(c)]. However, in Figs. 4(b) and 4(d) for $\alpha = 2.8$, we note the repulsion that exists between the wave packet and the lattice solitonic profile. We can see in Fig. 4(b) that the largest part of the wave function moves to the negative side while most of the lattice deformation [see Fig. 4(d)] goes to the positive side. In Fig. 5(a), we graph, for a wide range of α, the mean distance between the magnon and the lattice deformation (i.e., $|\langle n_S\rangle - \langle n_L\rangle|$). The long-time behavior of the magnon and lattice deformation mean positions were computed as $\langle n_S\rangle = \langle n\rangle_S(t \to 4 \times 10^3)$ and $\langle n_L\rangle = \langle n\rangle_L(t \to 4 \times 10^3)$. In Fig. 5(b) we plot the velocity of both magnon's excitation and the lattice deformation versus α (V_S and V_L in Fig. 5(b)]. Calculations of the velocity were done by estimating the slope of the quantities $\langle n\rangle_S(t)$ and $\langle n\rangle_L(t)$ at the long-time limit. It suggests that the magnon and the lattice deformation kept approximately the same position and velocity only for $\alpha \approx 0.38(2)$. For other α values, we observe that the magnon and the lattice deformation have distinct velocity and are kept completely separated.

The magnon-lattice pair formation was only noticed for a tiny range of α values [around roughly 0.38(2)]; it is a new and

counterintuitive result, thus deserving a more detailed discussion. In general, we do not have a quantitative description that definitely explains this key issue. However, we can, at least, try to point out the main difference between the magnetic case considered here and the previous electronic case reported in Refs. [21,26]. In the electronic context, it was numerically and analytically proved that electron-lattice pair formation exists in a wide range of values of electron-lattice coupling [21,26]. In this case, only the hopping term (the kinetic energy) depends on the effective coupling with the lattice deformation. For the one-magnon subspace, both the effective potential energy and the effective kinetic energy depend on the mass displacements. The antigenic effects between both potential and kinetic energies on the magnetic model seem to be the key ingredient behind the special kind of magnon-lattice pair formation we have found.

IV. SUMMARY AND FINAL STATEMENT

In this work we considered the one-magnon subspace of a quantum Heisenberg Hamiltonian with ferromagnetic ground state. Within our theoretical formalism we considered the cubic interaction along the spin chain and the interaction between the magnon's excitation and the spin vibrations as a function of the distance between the spins. We found the numerical solution of the quantum and classical dynamics equations. Our calculations indicate that the magnon-lattice coupling promotes distinct dynamics in this nonlinear model. For a tiny range of values of the magnon-lattice coupling, we found a magnon-soliton pair similar to the electron-soliton pair that was found in Refs. [19,21]. We also numerically demonstrated that the magnon-soliton pair formation is a rare event that happens only for a narrow range of α values. In general, our calculations suggest that the magnon-lattice coupling effectively promotes a repulsion between the magnon and the solitonic deformation that exists within this nonlinear chain. We emphasize that in our model we dealt with a special kind of time-dependent disorder distribution at the hopping terms. Despite the fact that our work does not contain a static disorder similar to what exists in the standard Anderson model, the magnon-lattice interaction at the spin-spin coupling represents a dynamic disorder within the system. We hope that the magnon dynamics obtained and its direct relation with the magnon-lattice coupling stimulate further investigation.

[1] B. Kramer and A. MacKinnon, Rep. Prog. Phys. **56**, 1469 (1993).

[2] E. Abrahams, P. W. Anderson, D. C. Licciardello, and T. V. Ramakrishnan, Phys. Rev. Lett. **42**, 673 (1979).

[3] S. N. Evangelou and D. E. Katsanos, Phys. Lett. A **164**, 456 (1992).

[4] F. A. B. F. de Moura, M. D. Coutinho-Filho, E. P. Raposo, and M. L. Lyra, Phys. Rev. B **66**, 014418 (2002)

[5] M. Johansson, M. Hörnquist, and R. Riklund, Phys. Rev. B **52**, 231 (1995).

[6] P. K. Datta and K. Kundu, Phys. Rev. B **53**, 14929 (1996).

[7] S. Tietsche and A. Pikovsky, Europhys. Lett. **84**, 10006 (2008).

[8] M. O. Sales, W. S. Dias, A. Ranciaro Neto, M. L. Lyra, and F. A. B. F. de Moura, Solid State Commun. **270**, 6 (2018).

[9] S. Flach, D. O. Krimer, and Ch. Skokos, Phys. Rev. Lett. **102**, 024101 (2009).

[10] T. V. Laptyeva, J. D. Bodyfelt, and S. Flach, Europhys. Lett. **98**, 60002 (2012).

[11] M. V. Ivanchenko, T. V. Laptyeva, and S. Flach, Phys. Rev. Lett. **107**, 240602 (2011).

[12] C. Skokos, I. Gkolias, and S. Flach, Phys. Rev. Lett. **111**, 064101 (2013).

[13] B. J. Alder, K. J. Runge, and R. T. Scalettar, Phys. Rev. Lett. **79**, 3022 (1997).

[14] L. S. Brizhik and A. A. Eremko, Physica D **81**, 295 (1995).

[15] O. G. Cantu Ross, L. Cruzeiro, M. G. Velarde, and W. Ebeling, Eur. Phys. J. B **80**, 545 (2011).

[16] M. G. Velarde and C. Neissner, Int. J. Bifurcation Chaos **18**, 885 (2008).

[17] M. G. Velarde, W. Ebeling, and A. P. Chetverikov, Int. J. Bifurcation Chaos **21**, 1595 (2011).

[18] A. P. Chetverikov, W. Ebeling, and M. G. Velarde, Eur. Phys. J. B **80**, 137 (2011).

[19] D. Hennig, M. G. Velarde, W. Ebeling, and A. Chetverikov, Phys. Rev. E **78**, 066606 (2008).

[20] M. G. Velarde, W. Ebeling, and A. P. Chetverikov, Int. J. Bifurcation Chaos **15**, 245 (2005).

[21] M. G. Velarde, J. Comput. Appl. Math. **233**, 1432 (2010).

[22] M. G. Velarde, W. Ebeling, and A. P. Chetverikov, Eur. Phys. J. B **85**, 291 (2012).

[23] W. Ebeling, A. P. Chetverikov, G. Röpke, and M. G. Velarde, Contrib. Plasma Phys. **53**, 736 (2013).

[24] A. P. Chetverikov, W. Ebeling, and M. G. Velarde, Eur. Phys. J.: Spec. Top. **222**, 2531 (2013).

[25] A. Ranciaro Neto, M. O. Sales, and F. A. B. F. de Moura, Solid State Commun. **229**, 22 (2016).

[26] A. Ranciaro Neto and F. A. B. F. de Moura, Commun. Nonlinear Sci. Numer. Simul. **40**, 6 (2016).

[27] F. A. B. F. de Moura, Int. J. Mod. Phys. C **22**, 63 (2011).

[28] E. Hairer, S. P. Nørsett, and G. Wanner, *Solving Ordinary Dierential Equations I: Nonstiff Problems*, Springer Series in Computational Mathematics, 2nd revised. ed. (Springer-Verlag, New York, 1993); W. H. Press, B. P. Flannery, S. A. Teukolsky, and W. T. Wetterling, *Numerical Recipes: The Art of Scientific Computing*, 3rd ed. (Cambridge University Press, New York, 2007).

[29] N. F. Smyth and A. L. Worthy, Phys. Rev. E **60**, 2330 (1999).